PERGAMON

International Journal of Heat and Mass Transfer 42 (1999) 3563–3573

International Journal of HEAT and MASS TRANSFER

www.elsevier.com/locate/ijhmt

Enhancement of liquid forced convection heat transfer in microchannels due to the release of dissolved noncondensables

T.M. Adams, S.M. Ghiaasiaan*, S.I. Abdel-Khalik

G. W. Woodruff School of Mechanical Engineering, Georgia Institute of Technology, Atlanta, GA 30332-0405, USA

Received 8 October 1998; received in revised form 4 January 1999

Abstract

An experimental investigation addressing the effect of the release of dissolved noncondensables on the heat transfer in a long, heated microchannel subject to subcooled liquid forced convection was conducted. The convection heat transfer coefficients near the exit of a copper microchannel with 0.76 mm inner diameter and 16 cm heated length, subject to forced-flow cooling by subcooled water, were measured. The range of experimental parameters were: wall heat flux = 0.5–2.5 MW/m^2; liquid velocity = 2.07 to 8.53 m/s; channel exit pressure = 5.9 bar. Experiments were performed with degassed water and water saturated with air.

The convection heat transfer coefficients obtained with degassed water were systematically under predicted by the widely-used Dittus–Boelter correlation for turbulent pipe flow. The presence of dissolved air in water could increase the heat transfer coefficients by as much as 17%, despite the fact that the maximum increase in the coolant velocity due to the noncondensable gas release was only a few percent. The heat transfer enhancement increased with increasing the heat flux and decreasing the liquid velocity.

Keywords: Microchannel; Forced convection; Noncondensables; Two-phase flow; Heat transfer; Enhancement; Void fraction

1. Introduction

Microchannels with $D_H \approx O$ (1 mm) are utilized in a variety of applications, including micro-electronic cooling, and miniature refrigeration and heat exchanger systems. The characteristic length scales in these microchannels are typically orders of magnitude larger than the fluid molecular mean free path. They, therefore, do represent microscale transport characteristics [1] and their laminar flow phenomena are well-predicted by continuum theoretical models [2,3]. The hydrodynamic and heat transfer processes associated with turbulent flow in microchannels, however, are known to be different from large channels and are poorly understood. The disagreement between turbulent characteristics of microchannels with known characteristics of turbulent flow in larger channels has been attributed by some investigators to the possibility that the predominant turbulent eddies in microchannels may have characteristic lengths of the order of the microchannel diameters [4]. Well-known correlations for turbulent friction factor and convection heat transfer appear to do poorly when applied to microchannels [5–8]. The available experimental data are inconsistent with

* Corresponding author. Tel.: (404) 894-3746; fax: (404) 894-3733.

E-mail address: sered.ghiaasiaan@me.gatech.edn (S.M. Ghiaasiaan)

0017-9310/99/$ - see front matter
PII: S0017-9310(99)00023-X

Nomenclature

A_w	wall cross-sectional area [m^2]
C_{PL}	specific heat of liquid [J/kg K]
C_{He}	Henry's coefficient [Pa]
D	channel diameter [m]
D_H	hydraulic diameter [m]
G	mass flux [kg/m^2 s]
g	gravitational acceleration [m/s^2]
h	convection heat transfer coefficient [W/m^2 K]
$\hat{h}$	specific enthalpy [J/kg]
K_{ex}	test section exit loss coefficient
k	thermal conductivity [W/m K]
L	channel length [m]
M	molecular mass [kg/k-mole]
$\dot{m}_L$	liquid mass flow rate [kg/s]
Nu	Nusselt number ($=hD/k$)
P	pressure [Pa]
Pr	Prandtl number ($=\mu Cp/k$)
q''	wall heat flux [W/m^2]
R_n	noncondensable gas constant [N m/kg K]
Re	Reynolds number
T	temperature [K]
X	noncondensable mole fraction
x	noncondensable mass fraction
z	axial coordinate [m]

Greek symbols

α	void fraction
θ	angle of inclination with respect to the horizontal plane [R]
μ	dynamic viscosity [kg/ms]
ξ	dimensionless parameter representing disequilibrium
Φ_{L0}	two-phase multiplier
ρ	density [kg/m^3]

Subscripts

G	vapor–noncondensable gas mixture
h	homogeneous
in	channel inlet
n	noncondensable
sat	saturation
TP	two-phase
v	vapor
w	wall
1	axial location of thermocouples near channel inlet
2	axial location of thermocouples near channel exit
∞, 2	downstream of the test section exit

respect to the major trends, however. Some recent investigations indicate that the turbulent wall friction factors in smooth microchannels are lower than the predictions of widely-used correlations [8,9] and this observation is consistent with the aforementioned argument regarding the suppression of turbulent eddies due to the small channel characteristic dimension [4]. With regards to convection heat transfer, however, the available data are inconsistent. Some investigators have observed that the widely-used turbulent forced convection heat transfer correlations under predict the heat transfer in microchannels [5–6], while others have

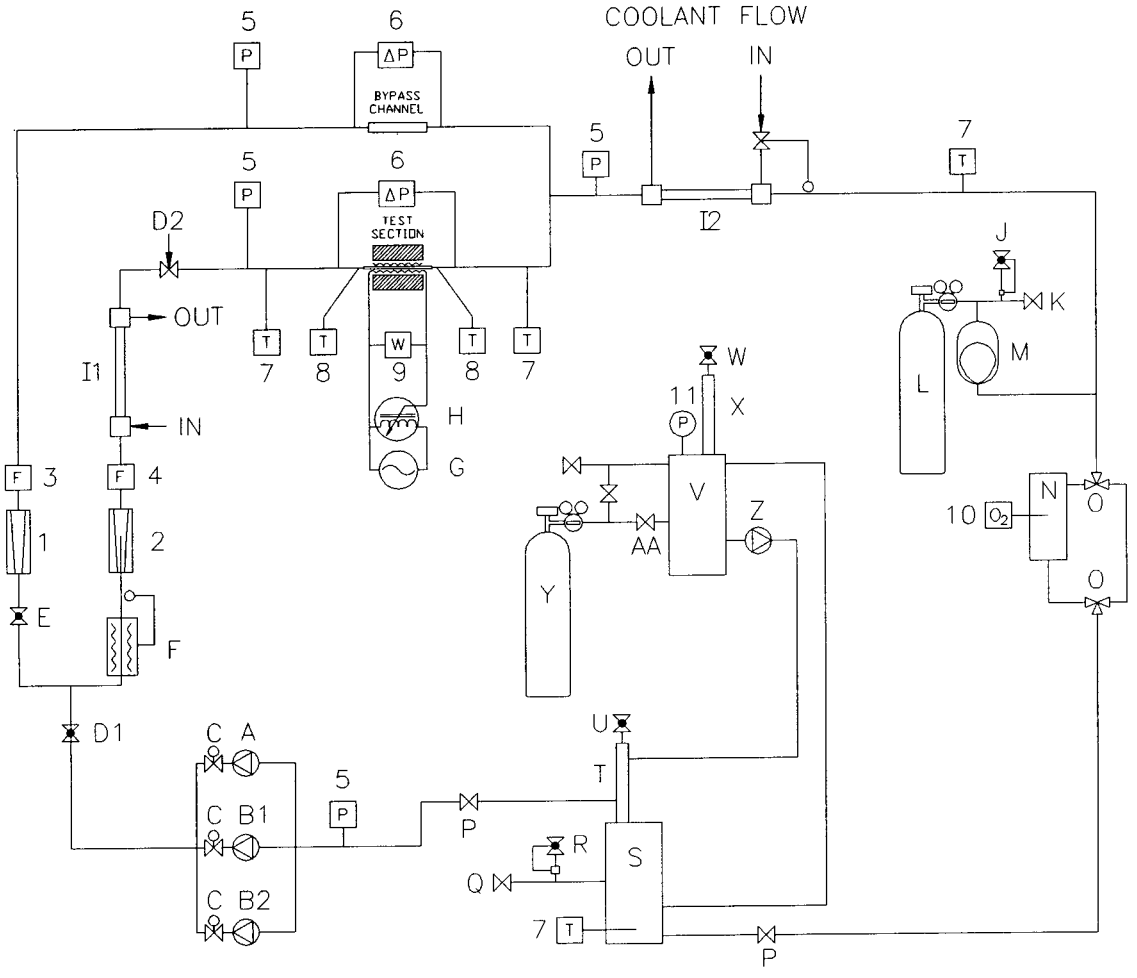

Fig. 1. The test loop.

reported the opposite [7]. Direct experimental measurement of microchannel turbulent characteristics, e.g., the turbulent velocity profiles, are evidently needed.

An issue related to the forced flow of liquids in microchannels, which is often of negligible consequence in large channels, is the impact of the noncondensables dissolved in the liquid. Dissolved noncondensables usually undergo little release in large channels. In microchannels, however, due to the typically large axial pressure gradients, significant desorption of dissolved noncondensables may take place, leading to the development of a gas–liquid two-phase flow with enhanced velocity and convection heat transfer characteristics.

The gas–liquid two-phase forced convection heat transfer has been studied in the past rather extensively, as reviewed in [10,11]. More recent studies include [12,13]. The bulk of the previous studies, however, dealt with the developed flow of a liquid–gas mixture, where the velocity enhancement in the liquid due to mixing with the gas augmented the convection heat transfer. In fully-developed two-phase flow, however, the enhancement is modest for small void fractions [10,11]. More significant enhancement is observed at low liquid velocities and when the gas is injected through the channel wall. The gas injection through the wall, which has some similarity with the noncondensable gas release into bubbles nucleating on channel wall crevices [14], disrupts the boundary layer and augments turbulence, both of which contribute to the enhancement of convection heat transfer.

In a recent study, Adams et al. [15] analytically assessed the impact of the desorption of dissolved nitrogen and argon in water on the flow phenomena in heated microchannels with $D = O$ (0.1–1 mm), and $L/D = 200$, using a homogeneous-equilibrium model. Their results indicated that significant voidage can develop in microchannels while the liquid flowing in

Table 1
Experimental system hardware components

Part letter	Name of part
A	Centrifugal pump
B1	Seepex positive displacement pump
B2	Micropump positive displacement pump
C	Pump exit ball valves
D1	System flow control throttling valve
D2	Test section inlet metering valve
E	Bypass control throttling valve
F	Test section in-line heater
G	208 VAC power supply
H	Variac
I1	Test section counter flow heat exchanger
I2	Counter flow heat exchanger
J	Pressure operated relief valve
K	Manually operated relief valve
L	Nitrogen cylinder
M	Teflon bellows accumulator
N	Dissolved oxygen sensor housing
O	Three way valves
P	Tank isolation ball valves
Q	Supply water inlet port valve
R	Peristaltic pump relief valve
S	Degassing/feed water tank
T	Noncondensable catching vertical column
U	Degassing tank relief valve
V	Saturation tank
W	Saturation tank relief valve
X	Vertical filter column
Y	Compressed air cylinder
Z	Recirculation pump
1	Rotameter
2	Rotameter
3	Liquid flow transducer
4	Liquid flow transducer
5	Pressure transducer
6	Diff pressure transducer
7	Thermocouple
8	Thermocouple
9	Wattmeter
10	Dissolved oxygen probe

them is subcooled, in particular under low liquid flow rate and high heat flux conditions.

In this paper we report on an experimental study of the impact of dissolved noncondensables on convective heat transfer in a heated microchannel subject to subcooled liquid forced flow. Experiments are performed in a uniformly-heated channel 0.76 mm in diameter and with 16-cm heated length, using degassed water and water saturated with air at the inlet to the test section. The convection heat transfer enhancement at the test section exit due to the presence of the dissolved noncondensables is quantified and its dependence on flow and system parameters is examined. The two-phase flow parameters resulting from the release of the dissolved noncondensables are calculated using solubility and equilibrium limit characteristics. It is argued that the existing correlations for gas–liquid forced convection heat transfer significantly underestimate the heat transfer enhancement that results from the noncondensable release, indicating the need for further systematic studies.

2. Experimental

Fig. 1 is a schematic of the main experimental test loop. Important hardware (items labeled with letters) and instrumentation (items labeled numerically) are listed in Table 1. The flow loop is a flexible system for experiments on various aspects of microchannel thermal-hydraulics.

The test loop includes two parallel lines, one including the test section and the other providing a low resistance bypass. Water flow rates over a wide range can be provided using three different pumps, A, B_1 and B_2 and flow rates through the test section and the bypass lines can be finely controlled using the throttle valves D_1 and E. In the experiments reported here, however, the bypass line was isolated by maintaining valve E closed.

Details of the test section are displayed in Fig. 2. The test section inner diameter was 0.76 mm, and was constructed from free-machining copper (tellurium copper, C 14500), using the EDM machining technique with extreme care to ensure accurate dimensions. The surface roughness and diameter of the test section were measured by cutting separate manufactured samples and placing them in a profilemeter. The mean surface roughness was 2 μm and the estimated standard deviation representing the uncertainty in channel diameter was only 2.5 μm. Heat input to the test section was provided by an insulated 20 AWG (0.89 mm outer diameter) NiChrome wire wrapped helically around the test section in a tight fashion, at 20 turns per 2.5 cm.

Six Type E stainless steel-sheathed thermocouples were installed in the test section. Three thermocouples were rigidly inserted, 120° apart, to a depth of 0.25 mm from the inner channel wall, at an axial location 4.25 cm from the test section inlet (1.25 cm from the inlet to the heated segment). Another three thermocouples were inserted in an identical fashion at 4.25 cm from the test section exit (1.25 cm from the exit of the heated segment). The axial locations of these two groups of thermocouples will be referred to as z_1 and z_2, respectively. Using these thermocouple readings, the test section inner wall temperatures at z_1 and z_2 could be calculated based on one-dimensional radial conduction. Axial conduction is insignificant when [16]:

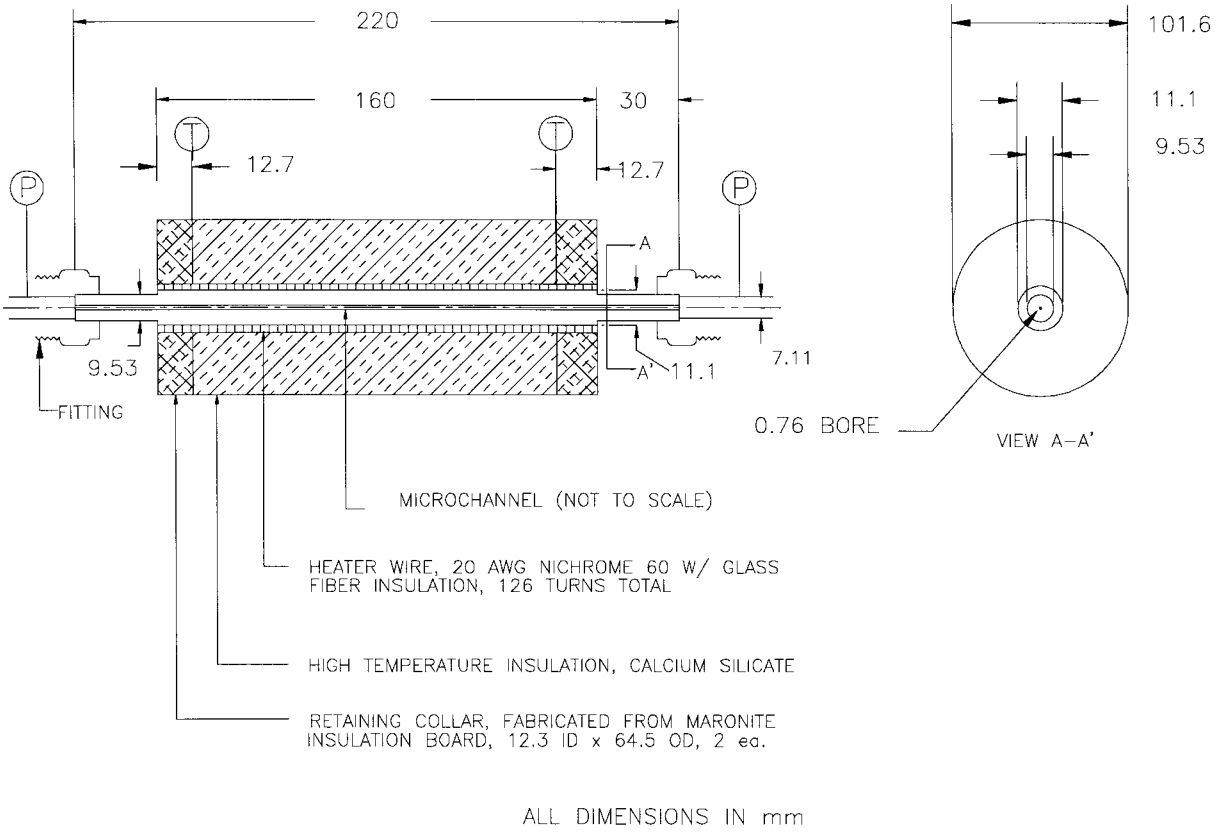

Fig. 2. The test section.

$$\frac{k_w A_w}{L\dot{m}_L C_{PL}} < 0.005 \tag{1}$$

For our test section the magnitude of the above parameter is about 0.0045. Heat losses due to conduction through the test section ends were also estimated, and were found to be negligible.

The test section depicted in Fig. 2 was attached to tubes with approximately 7.1 mm inner diameters at both ends. Using pressure transducers with ±3.4 kPa accuracy, the pressures at the inlet and outlet of the test section and at the suction of the pump, were all measured. In addition, a differential pressure transducer measured the pressure drop across the test section. The pressure taps were all connected to the aforementioned 7.1 mm diameter tubes near the test section entrance and exit. All experiments were performed under steady-state conditions. The test section exit pressure and inlet temperature were maintained constant in all the tests at 590 ± 5 kPa and 50 ± 1.5°C, respectively. More details can be found in [17].

3. Analysis

The convection heat transfer coefficient at z_2, corresponding to the location of the thermocouples near the exit of the test section (see Fig. 2) can be found from:

$$h_2 = \frac{q''}{T_{w2} - T_{L2}} \tag{2}$$

The state of the coolant fluid at z_2, furthermore, can be calculated from an energy balance on the test section:

$$G\left[\left(\hat{h} + \frac{G^2}{2\rho^2}\right)_2 - \left(\hat{h} + \frac{G^2}{2\rho^2}\right)_{in}\right] = \frac{4q''}{D}(z_2 - z_m) \tag{3}$$

In experiments with degassed water $\hat{h} = \hat{h}_L$ and $\rho = \rho_L$ everywhere, with $\hat{h}_L$ and ρ_L representing the local liquid properties, and Eq. (3) can be solved for $\hat{h}_{L,2}$. (Note that the dependence of ρ_L on $\hat{h}_L$, and from there

on T_L, is considered.) From there T_{L2} can be readily calculated.

To obtain the fluid state at z_2 when noncondensable release takes place, the following assumptions are made: (1) the concentration of the noncondensable in the liquid is small such that the liquid properties are not affected by the presence of the noncondensable; (2) the effect of the noncondensable heat of desorption is negligible; (3) the gas pockets (bubbles) formed due to the release of the noncondensable are everywhere saturated with respect to vapor concentration; (4) the noncondensable is an ideal gas; and (5) the two-phase flow resulting from the release of the noncondensable gas is in a homogeneous-equilibrium state everywhere. Assumptions 1 and 2 are appropriate due to the very small solubility in water of noncondensables of interest here. Assumption 3 represents an upper estimate of the evaporation that accompanies the release of the dissolved noncondensables. Assumption 4 is evidently reasonable. Assumption 5 is based on the relatively extensive experimental observations regarding gas–liquid two-phase flow in microchannels, where in unseparated (bubbly, slug and churn) flow regimes the gas–liquid slip velocity is suppressed by surface tension [18,19]. Although the two-phase flow regimes were not directly observed in this study, based on the magnitude of phasic superficial velocities, the two-phase flow patterns are believed to have been bubbly in all cases.

The noncondensable species mass and the mixture energy conservation equations can then be written as [15]:

$$\frac{\mathrm{d}}{\mathrm{d}z}\left\{\frac{G}{\rho_h}[\rho_L(1-\alpha)x_L+\rho_n\alpha]\right\}=0 \tag{4}$$

$$\frac{\mathrm{d}}{\mathrm{d}z}\left\{\frac{2}{\rho_h}\left[\rho_L(1-\alpha)\hat{h}_L+\rho_v\alpha\hat{h}_v+\frac{G^2}{2\rho_h}\right]\right\} = -Gg\ \sin\ \theta+\frac{4q''}{D} \tag{5}$$

where

$$\rho_h=\alpha\rho_G+(1-\alpha)\rho_L \tag{6}$$

$$\rho_G=\rho_v+(P-P_{sat})(T)/(R_nT) \tag{7}$$

The noncondensable mole fraction in the liquid is represented as:

$$X_L=\frac{P-P_{sat}}{C_{He}\xi} \tag{8}$$

where $0\leqslant\xi\leqslant1$ is a parameter that represents the nonequilibrium between the gas and liquid phases with respect to the concentration of the noncondensable. With $\xi=1$, Eq. (8) represents Henry's law and implies equilibrium. Therefore, $\xi=1$ is an upper limit with respect to the release of noncondensables. Since typically $X_L\ll1$, Eq. (8) can be manipulated to get:

$$x_L=\frac{M_n}{X_LM_n+(1-X_L)M_v}X_L\approx\frac{M_n}{M_v}\frac{P-P_{sat}}{C_{He}\xi} \tag{9}$$

Using the above relations, Eqs. (4) and (5) can be integrated from z_{in} to z_2 to get:

$$\frac{1}{\rho_{hz}}\left[\rho_L(1-\alpha)\frac{M_n}{M_v}\frac{P-P_{sat}}{C_{He}\xi}+\alpha\frac{P-P_{sat}}{R_nT_L}\right]_2=x_{L,in} \tag{10}$$

$$\left\{\frac{G}{\rho_h}\left[\rho_L(1-\alpha)\hat{h}_L+\rho_v\alpha\hat{h}_v+\frac{G^2}{2\rho_h}\right]\right\}_2 - G\left[h_L+\frac{G^2}{2\rho_L^2}\right]_{in}=\frac{4q''}{D}(z_2-z_{in}) \tag{11}$$

Knowing the pressures at the channel inlet and at z_2 (from pressure measurements, assuming a linear pressure distribution) and utilizing appropriate property tables, Eqs. (10) and (11) can be iteratively solved for α_2 and $T_{L,2}$.

As mentioned in Section 2, pressure measurements were made at locations immediately upstream and downstream of the test section inlet and exit (Fig. 2). The pressure at the test section exit, P_{ex}, is related to the pressure downstream of the test section exit, $P_{\infty,2}$, according to:

$$P_{ex}=P_{\infty,2}+(K_{ex}-1)\frac{G^2}{2\rho_{L,ex}}\Phi_{L0} \tag{12}$$

However, since $K_{ex}\approx1$ for an infinitely large flow area expansion [20], $P_{ex}\approx P_{\infty,2}$. Also, note that no correction for the inlet pressure loss is needed, since $x_{L,in}$ in Eq. (10) represents the known noncondensable mass fraction at inlet, and $[h_L+G^2/2\rho_L]_{in}$ represents the stagnation enthalpy of the fluid at inlet, which is equal to the stagnation enthalpy of the fluid before it enters the test section, and is not affected by the entrance pressure loss.

With noncondensables present, the convection heat transfer coefficient can be calculated from Eq. (2) in two ways: by using $T_{L,2}$ found from Eq. (3), i.e., based on an energy balance which neglects the noncondensable release; or by using T_2 provided by Eqs. (10) and (11). For the results presented in this paper, however, the difference between the two methods was negligible. Values of C_{He} as a function of temperature were obtained from [21].

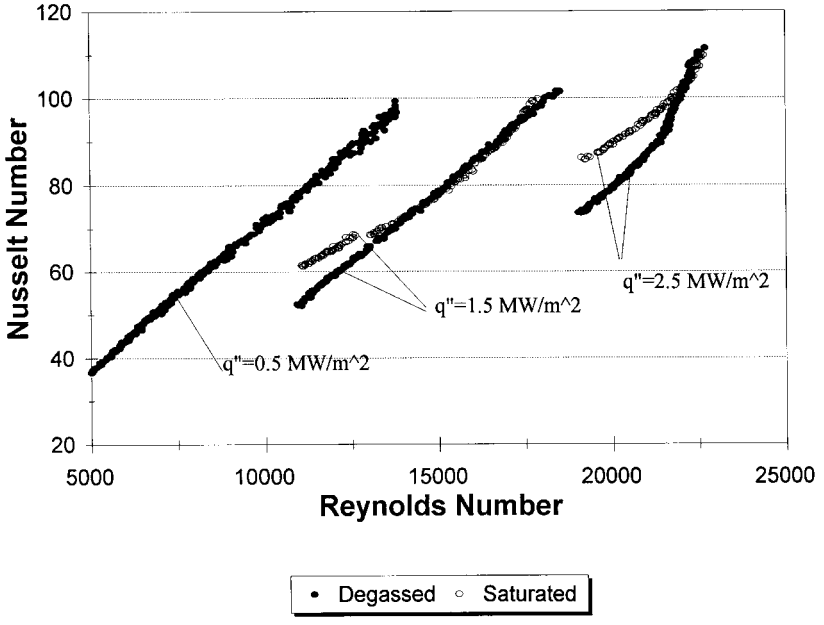

Fig. 3. The enhancement in $Nu_{L,2}$ due to the presence of dissolved air.

4. Results and discussion

Experiments were performed at three different heat fluxes: 0.5, 1.5 and 2.5 MW/m^2. For each heat flux a large number of tests were carried out covering channel mass fluxes in the 1998 to 8352 kg/m^2 s range, corresponding to $Re_L = 5000$–23,000, with $Re_L = GD/\mu_L$. In all the tests, the water temperature at inlet to the test section was 50 ± 1.5°C and the pressure at the test section exit was 590 ± 5 kPa.

The experimental Nusselt numbers representing the axial location z_2 for $q'' = 0.5$, 1.5 and 2.5 W/m^2 are

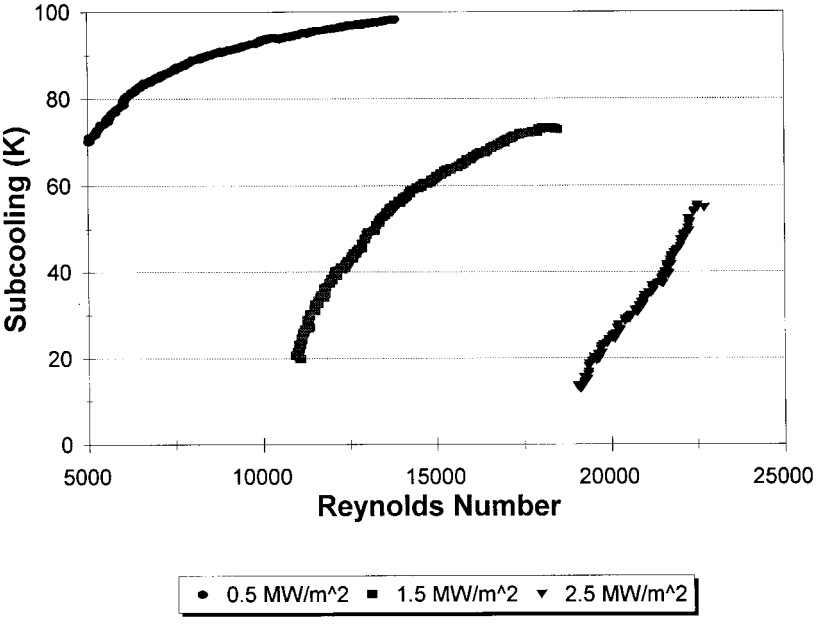

Fig. 4. Bulk liquid subcooling at z_2.

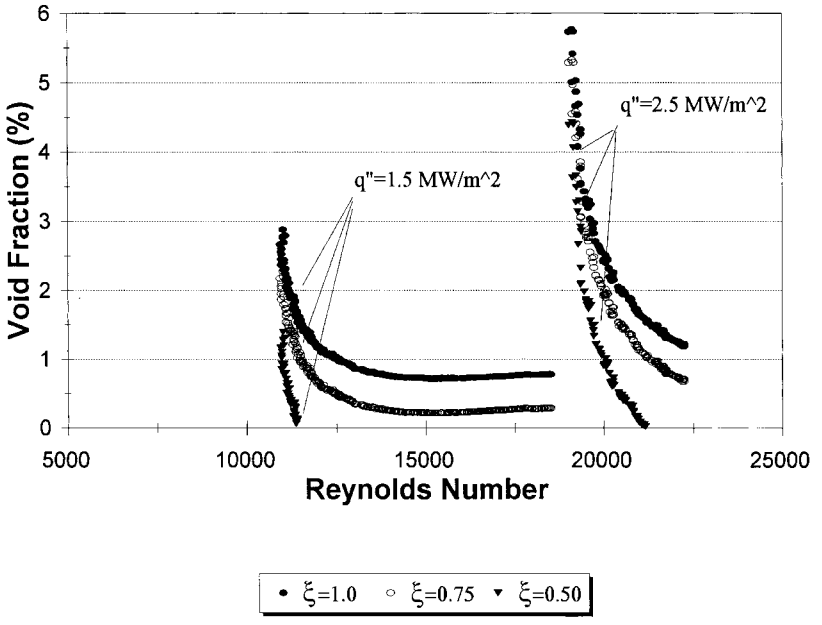

Fig. 5. Void fraction at z_2 caused by the air desorption.

depicted in Fig. 3, as a function of Re_L. For the three depicted heat fluxes the experiments covered different mass flux ranges. This was necessary in view of the similar liquid temperature variations among the three sets of experiments. The depicted results, while indicating that the dissolved air generally enhances the convection heat transfer coefficient, also show that the level of enhancement depends on the mass flux (or Re_L), as well as on the imposed heat flux, q''. These trends in fact represent the dependence of the results on the pressure drop and the increase of the liquid temperature in the test section. They can therefore be

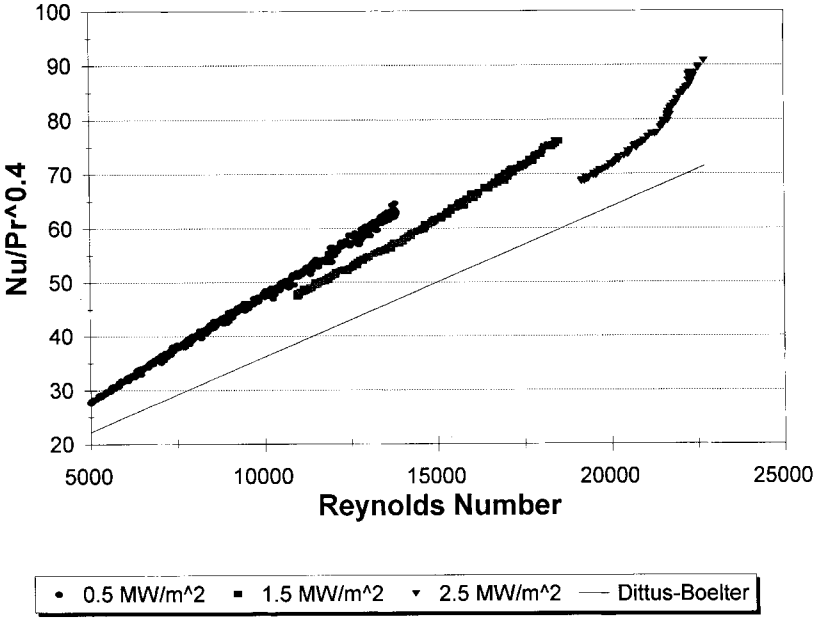

Fig. 6. Variation of $(Nu/Pr)_{L,2}$ with Re_L for degassed water.

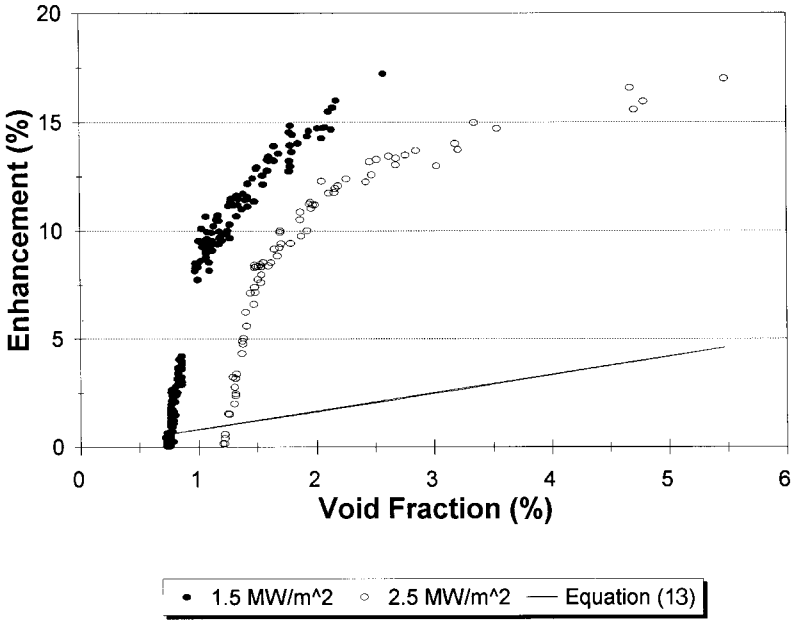

Fig. 7. The enhancement in $Nu_{L,2}$ caused by the desorption of air as a function of the maximum void fraction at z_2.

better understood by examining Figs. 4 and 5, which depict the variations of local bulk liquid subcooling, $T_{sat} - T_L$, and void fraction, α, at z_2, as functions of Re_L. Since the water at inlet to the test section is approximately saturated with air, a reduction of pressure and an increase in temperature of the liquid both lead to the release of the dissolved air. This is because the solubility of air in water increases with increasing the pressure and decreasing the temperature. The effect of the temperature increase is by far more significant in the depicted results, however. As the mass flux (or equivalently Re_L) is increased, the fluid temperature variation in the test section is decreased, leading to lower noncondensable release at z_2. The void fractions depicted in Fig. 5 were calculated with $\xi = 0.5$, 0.75 and 1 and support the aforementioned explanation. The magnitude of the void fraction is of course sensitive to ξ, and $\xi = 1$, which represents equilibrium between the liquid and gas phases with respect to the concentration of air, provides the upper limit for void fraction. With $q'' = 0.5$ MW/m^2, due to the relatively small liquid velocities, the pressure drops in the test section were small, and led to insignificant noncondensable release. The presence of dissolved air in experiments with $q'' = 0.5$ MW/m^2 thus caused negligible enhancement in the convection heat transfer coefficients. The sharp increase in α at low Re_L is a result of approaching the saturation temperature of the liquid, which leads to significant evaporation. The experimental $Nu_L/Pr_L^{0.4}$ values at z_2, obtained with degassed water, are depicted in Fig. 6 as a function of Re_L, where the predictions of the Dittus and Boelter correlation [22] are also displayed. Evidently the correlation under predicts the data systematically and significantly. This is consistent with previously reported experimental observations [5,6], and confirms that the turbulence characteristics in microchannels may be significantly different than in larger channels.

The variations of the heat transfer coefficient (or Nusselt number) enhancements caused by the presence of dissolved air, as a function of the void fraction at z_2, are depicted in Fig. 7. Forced convection in two-component two-phase flow has been extensively studied in the past, as reviewed in [10–13]. The wall heat transfer, like all other important thermal-hydraulic processes, is a strong function of the two-phase flow regime. Furthermore, in developing flow situations with gas injection it strongly depends on the gas injection method. In our experiments, in view of the low void fractions and based on the existing experimental data dealing with the two-phase flow regimes in microchannels [18,19], dispersed bubbly flow appears to be the only feasible two-phase flow regime. In a developed bubbly flow regime heat convection between the wall and the liquid is the predominant heat transfer mechanism and consequently [10,11]:

$$Nu_{TP}/Nu_L \approx (1-\alpha)^{-n} \tag{13}$$

where n represents the power of Reynolds number in the appropriate single-phase forced convection correlation $Nu = f(Re, Pr)$. Eq. (13), as noted in Fig. 7, is

utterly inadequate for our experimental results. The results of our experiments clearly show that the increase in the coolant velocity is not the predominant heat transfer enhancement mechanism associated with the release of dissolved noncondensables. The heat transfer enhancement is likely to be, at least partially, due to the formation and release of small bubbles on the channel walls. Experimental studies in the past have indicated that the injection of a gas through channel walls into liquid can enhance heat transfer rather significantly [23,24]. This heat transfer augmentation is primarily due to the disruption of the thermal boundary layer and the generation/augmentation of local turbulence. The formation and release of gas bubbles due to the desorption of noncondensables on channel walls may resemble the formation and release of vapor bubbles in nucleate boiling, where the generated bubbles enhance the wall-fluid sensible heat transfer [25,26]. The clarification of the heat transfer mechanism in microchannels caused by the release of dissolved gases evidently needs more systematic experimental studies.

5. Conclusion

The impact of dissolved noncondensables on the convection heat transfer coefficient in microchannels subject to subcooled forced-flow cooling was experimentally studied. The experiments were carried out in a uniformly heated copper microchannel 0.76 mm in diameter and 16 cm in heated length, over the following parameter ranges: velocity = 2.07–8.53 m/s; wall heat flux = 0.5–2.5 MW/m^2; channel inlet pressure = 600–886 kPa; channel exit pressure = 590 kPa. The impact of dissolved air was examined by performing similar experiments with degassed water and with water saturated with air at the inlet to the test section. The convection heat transfer coefficients at a point 1.25 cm upstream from the exit of the heated segment of the test section were measured in all the tests.

With degassed water, the measured heat transfer coefficients were monotonically and significantly higher than the predictions of widely-used correlations for turbulent pipe flow. The presence of dissolved air, furthermore, increased the measured heat transfer coefficients by as much as 17%. The enhancement in the heat transfer coefficient increased with increasing the wall heat flux and with decreasing the liquid mass flux, both of which lead to increasing the change in the coolant temperature as it flows in the heated channel. The maximum void fraction in the channel resulting from the desorption of the dissolved air, which was calculated by assuming local equilibrium, was only a few percent, however.

The mechanism responsible for the augmentation of heat transfer resulting from the presence of noncondensables is not known and further investigations are recommended.

References

[1] C.-L. Tien, A.M. Berlin, Microscale thermal phenomena in contemporary technology, J.X. An Jiaotong University 28 (1994) 9–30.
[2] E.P. Mikol, Adiabatic single and two-phase flow in small bore tubes, ASHRAE J. 5 (1963) 75–86.
[3] C.-O. Olsson, B. Sunden, Pressure drop characteristics of small-sized tubes, ASME Paper 94-WA/HT-1, 1994.
[4] S. Kakac, R.K. Shah, W. Aung, in: Handbook of Single Phase Convective Heat Transfer, John Wiley and Sons, New York, 1987, p. 42.
[5] W. Yu, R. Warrington, R. Barron, T. Ameel, An experimental and theoretical investigation of fluid flow and heat transfer in microtubes, Proc. ASME/JSME Thermal Eng. Conf. 1 (1995) 523–530.
[6] T.M. Adams, S.I. Abdel-Khalik, S.M. Jeter, Z.H. Qureshi, An experimental investigation of single-phase forced convection in microchannels, Int. J. Heat Mass Transfer 41 (1997) 851–859.
[7] B.X. Wang, X.F. Peng, Experimental investigation on liquid forced-convection heat transfer through microchannels, Int. J. Heat Mass Transfer 37 (1994) 73–82.
[8] C.-O. Olson, B. Sunden, Pressure drop characteristics of small-sized tubes, Paper presented in the ASME Winter Annual Meeting, Chicago, IL, 6–11 November 1994.
[9] J.E. Kennedy, G.M. Roach Jr, M.F. Dowling, S.I. Abdel-Khalik, S.M. Ghiaasiaan, S.M. Jeter, Z.H. Qureshi, The onset of flow instability in uniformly heated horizontal microchannels, J. Heat Transfer, submitted.
[10] J.C. Collier, in: Convective Boiling and Condensation, McGraw-Hill, New York, 1972, pp. 382–406.
[11] I. Michiyochi, Two-phase two-component heat transfer, in: Proc. 6th Nat. Heat Transfer Conference, Vol. 6, Hemisphere, Washington, DC, 1978, pp. 219–233.
[12] M.M. Shah, Generalized prediction of heat transfer during two-component gas–liquid flow in tubes and other channels, in: AIChE Symp. Series, , Vol. 77, 1981, pp. 140–151.
[13] K.S. Rezkallah, M.M. Vijay, G.E. Sims, A comparison of correlations of heat transfer coefficients in two-phase two-component gas–liquid flow in vertical tubes, in: Proc. 8th Nat. Heat Transfer Conf., Vol. 5, Hemisphere, Washington, DC, 1986, pp. 2349–2354.
[14] S.M. Ghiaasiaan, A.T. Wassel, A.A. Pesaran, Gas desorption from seawater in open-cycle ocean thermal energy conversion barometric upcomers, ASME J. Solar Energy Eng. 112 (1990) 204–215.
[15] T.M. Adams, S.M. Ghiaasiaan, S.I. Abdel-Khalik, Effect of dissolved noncondensables on hydrodynamics of microchannels subject to liquid forced convection, J. Enhanced Heat Transfer, accepted for publication.
[16] R.K. Shah, A.C. Mueller, Heat exchangers, in: W.M. Rolhsenow, J.P. Hartnett, E.N. Ganic (Eds.),

Handbook of Heat Transfer Applications, McGraw-Hill, New York, 1985, pp. 4.53–4.56.
[17] T.M. Adams, Turbulent convection in microchannels, PhD Thesis, G. W. Woodruff School of Mechanical Engineering, Atlanta, GA, 1998.
[18] K.A. Triplett, S.M. Ghiaasiaan, S.I. Abdel-Khalik, D.L. Sadowski, Gas–liquid two-phase flow regimes in microchannels. Part I: Two-phase flow regimes, Int. J. Multiphase Flow 25 (1999) 377–394.
[19] C.A. Damianides, J.W. Westwater, Two-phase flow patterns in a compact heat exchanger and in small tubes, in: Proc. 2nd UK National Conference on Heat Transfer, Glasgow, 14–16 September, 1988, pp. 1257–1268.
[20] T.R. Lahey, F.J. Moody, in: The Thermal-Hydraulics of a Boiling Water Nuclear Reactor, 2nd ed, American Nuclear Society, Lagrange Park, IL, 1993, p. 277.
[21] R.H. Perry, D.W. Green (Eds.), Perry's Chemical Engineers' Handbook, 6th ed., McGraw-Hill, New York, 1984, pp. 3–101.
[22] F.W. Dittus, L.M.K. Boelter, Heat transfer in automobile radiators of tubular type, University of California Publ. Eng. 2 (1930) 443–461 (reprinted from Nat. Comm. Heat Mass Transfer 12 (1985)).
[23] A.A. Kudirka, K.J. Gosh, P.W. McFadden, Two-phase heat transfer in a tube with gas injection from the walls, ASME Paper No. 65-HT-47, 1965.
[24] B.W. Martin, G.E. Sims, Forced convection heat transfer to water with air injection in a rectangular duct, Int. J. Heat Mass Transfer 14 (1971) 1115–1134.
[25] Y.Y. Hsu, R.W. Graham, Transport processes in boiling and two-phase systems, American Nuclear Society, LaGrange Park, IL, 1986.
[26] S. Van Stralen, in: Boiling Phenomena Physicochemical and Engineering Fundamentals and Applications, vols I and II, Hemisphere, Washington, DC, 1979.